









## RESEARCH ARTICLE

# Processing of polymer-derived, aerogel-filled, SiC foams for high-temperature insulation

Andrea Zambotti<sup>1</sup>  | Emanuel Ionescu<sup>2,3</sup>  | Nicola Gargiulo<sup>4</sup>  |  
Domenico Caputo<sup>4,5</sup>  | Cekdar Vakifahmetoglu<sup>6</sup>  | Balanand Santhosh<sup>1</sup>  |  
Mattia Biesuz<sup>1</sup>  | Gian Domenico Sorarù<sup>1,7</sup> 

<sup>1</sup>Department of Industrial Engineering, Glass and Ceramics Laboratory, University of Trento, Trento, Italy

<sup>2</sup>Institute of Materials Science, Darmstadt University of Technology, Darmstadt, Germany

<sup>3</sup>Fraunhofer Research Institution for Materials Recycling and Resource Strategy, Alzenau, Germany

<sup>4</sup>Center for Advanced Metrological and Technological Services (CeSMA), Federico II University of Naples, Napoli, Italy

<sup>5</sup>Department of Chemical, Materials and Industrial Production Engineering, Federico II University of Naples, Napoli, Italy

<sup>6</sup>Department of Materials Science and Engineering, Izmir Institute of Technology, Izmir, Turkey

<sup>7</sup>National Research Council Italy ICMATE CNR, Institute of Condensed Matter Chemistry and Technologies Energy, Genoa, Italy

## Correspondence

Andrea Zambotti, Department of Industrial Engineering, Glass and Ceramics Laboratory, University of Trento, Trento, Italy.

Email: [andrea.zambotti-1@unitn.it](mailto:andrea.zambotti-1@unitn.it)

## Funding information

Italian Ministry of University and Research, Grant/Award Number: PRIN2017 - 2017PMR932; AFOSR, Grant/Award Number: FA9550-21-1-0279

## Abstract

Porous polymer-derived ceramics (PDCs) are outperforming materials when low-density and thermal inertia are required. In this frame, thermal insulating foams such as silicon carbide (SiC) ones possess intriguing requisites for aerospace applications, but their thermal conductivity is affected by gas phase heat transfer and, in the high temperature region, by radiative mechanisms. Owing to the versatility of the PDC route, we present a synthesis pathway to embed PDC SiC aerogels within the open cells of a SiC foam, thus sensibly decreasing the thermal conductivity at 1000°C from 0.371 W·m<sup>-1</sup>K<sup>-1</sup> to 0.243 W·m<sup>-1</sup>K<sup>-1</sup>. In this way, it was possible to couple the mechanical properties of the foam with the insulating ability of the aerogels.

The presented synthesis was optimized by selecting, among acetone, n-hexane, and cyclohexane, the proper solvent for the gelation step of the aerogel formation to obtain a proper mesoporous colloidal structure that, after ceramization at 1000°C, presents a specific surface area of 193 m<sup>2</sup>·g<sup>-1</sup>. The so-obtained ceramic composites present a lowest density of 0.18 g·cm<sup>-3</sup>, a porosity of 90% and a compressive strength of 0.76 MPa.

## KEYWORDS

aerogel, cellular structure, polymer-derived ceramic, silicon carbide, thermal insulation

This is an open access article under the terms of the [Creative Commons Attribution](https://creativecommons.org/licenses/by/4.0/) License, which permits use, distribution and reproduction in any medium, provided the original work is properly cited.

© 2023 The Authors. *Journal of the American Ceramic Society* published by Wiley Periodicals LLC on behalf of American Ceramic Society.

## 1 | INTRODUCTION

High-temperature thermal insulation in aerospace and energy management fields is becoming more and more demanding, and with new challenges coming up, there is an exponential increase in the requirement for high-performing materials. In particular, the development of mechanically stable, hierarchically porous ceramics with very low density (for components like heat insulation panels) is one of the main research targets to reduce the net weight of aerospace vehicles and hence increase their overall performances.<sup>1</sup>

Similarly, cellular ceramics with controllable porosity and high specific surface area are attractive as catalyst supports, electrodes for batteries, sorbents for the removal of pollutants from water, and many other applications.<sup>2-5</sup> In these scenarios, thermal inertness and mechanical stability are the fundamental design features to ensure long-lasting performances. Accordingly, porous silicon carbide-based materials are among the most promising and appealing compounds.<sup>6-9</sup> These can be synthesized through partial sintering, direct foaming, replica methods, in situ growth or via polymer-derived ceramic (PDC) route.<sup>10-13</sup>

When considering high-temperature thermal insulation, ceramic aerogels are the most obvious solution. In these structures, thermal insulation is boosted by the fact that the mean free path of gas molecules is in the same dimensional range of pores, so that convection is dramatically reduced and conduction through particles bottlenecks remains the only effective heat transmission mechanism.<sup>14</sup> As temperature rises, radiative energy transfer becomes predominant according to the black-body radiation law, and in order to limit it, a good insulator should have an optical thickness larger than the mean free path of photons, in addition to low emissivity and high reflectance.<sup>15,16</sup>

In the broad manufacturing context of porous ceramics, the PDCs route is of particular interest: it allows obtaining ceramic foams and aerogels of different systems (e.g., SiOC, SiC, SiCN), with superior thermal stability, resistance to sintering and a reduced high temperature creep rate.<sup>12,17</sup> Moreover, even bulk PDCs possess low thermal conductivity,<sup>18,19</sup> and the presence of a free carbon phase in PDCs allows to reduce the thermal conductivity of the aerogels at high temperature, where the heat transfer is dominated by radiation, as they are substantially opaque to the electromagnetic radiation in the visible and near-infrared region.<sup>15</sup> However, PDCs aerogels possess two main drawbacks: their mechanical resistance is modest making their handling even more difficult in some cases, and they cannot be easily shaped, as they derive

from wet gels. On the other hand, ceramic foams can be easily obtained by the PDC route, have acceptable mechanical properties, but are substantially transparent to radiation due to the presence of large and continuous macropores.<sup>20-22</sup>

In this work, we present a silicon carbide structure, where the cells of a SiC foam obtained by replicating a polyurethane (PU) template are filled with a silicon carbide aerogel synthesized within the foam cells. The rationale behind the processing of such composite is to attain the synergy of the mechanical resistance provided by the low-density foam and the insulating properties of the aerogel. To allow for different pore size distributions in the aerogels and define the best aerogel/foam combination, both in term of porosity and compressive strength, we propose the use of three different solvents for the synthesis of the aerogel, namely acetone, n-hexane and cyclohexane, as in a previous work.<sup>23</sup>

## 2 | EXPERIMENTAL

### 2.1 | Impregnation of PU foams

Silicon carbide foams were prepared through the replica method following a published procedure.<sup>24</sup> Allylhydridopolycarbosilane StarPCS SMP-10 (Starfire Systems, Schenectady, NY, USA) was selected as preceramic polymer for the synthesis of silicon carbide, having an approximate formula corresponding to  $-\text{[SiH}_2\text{-CH}_2\text{]}_x\text{-[SiH(allyl)-CH}_2\text{]}_y\text{-}$  with a  $x:y = 9:1$  ratio and a reported ceramic yield of 72%–78%.<sup>25</sup> Flexible PU foams with an open cell structure, having a cell size of 90 pores per inch (PPI) were purchased from A.R.E. (Milan, Italy). According to the technical datasheet, the pore cell diameter is in the 440–520  $\mu\text{m}$  range with no closed cells. A 50/50 vol.% solution of acetone (Honeywell, CAS: 67-64-1) and n-hexane (Panreac, CAS: 110-54-3) was prepared for the solubilization of SMP-10 prior to the impregnation of the PU foams. In a typical impregnation, a 1:3 mass ratio between foam and SMP-10 was maintained, while the volume ratio between the solvent mix and the foam was kept to 1:5. To induce crosslinking by means of hydrosilylation of the vinyl groups of the polycarbosilane, 100  $\mu\text{l}$  of Karstedt's catalyst (Sigma-Aldrich, Saint Louis, MO, USA, CAS: 68478-92-2), diluted to 0.1% Pt in xylene, per gram of utilized SMP-10 were added to the polymer solution. The foams were manually impregnated till all the solution was absorbed by the foam. After a drying step of 24 h, these impregnated PU foams were subjected to a curing procedure at 300°C for 1 h under nitrogen.

## 2.2 | Processing of the aerogel-filled samples

Composite preceramic aerogel-foam architectures were produced by soaking the pretreated PU foam, impregnated with the preceramic polymer, inside the aerogel precursors solution and inducing the gel formation, followed by a controlled drying in supercritical CO<sub>2</sub>. The synthesis of the aerogel involved the crosslinking of SMP-10 in highly diluted conditions by adding divinylbenzene (DVB, Sigma Aldrich, CAS: 1321-74-0) as crosslinking agent, and 100  $\mu$ l of 0.1% Pt catalyst per gram of SMP-10. A molar ratio of 1 between silyl groups of SMP-10 and vinyl moieties of DVB was defined (i.e., 2.72 g of DVB per gram of polycarbosilane). A volume fraction of 80% of solvent was imposed to the precursors mix, selecting acetone, n-hexane and cyclohexane (Carlo Erba, CAS: 110-82-7) as separate organic solvents for the synthesis of the gels. It is known that organic solvents, depending on the solubility of the polymer within them, play a relevant role on the formation of colloidal structures, influencing both the dimensions of colloids and the pore size as a function of the swelling of the crosslinked polymer in the given solvent.<sup>23</sup> Therefore, the rationale behind the selection of the abovementioned solvents lies in our interest to define their effect on the final aerogel microstructure, particularly on the aerogel pore size and eventually on the overall shrinkage of the final aerogel with respect to that of the foam.

The steps of the composites fabrication are the following: (i) crosslinking of aerogel precursor mix with the pretreated foam, inside a Teflon liner sealed in a digestion vessel (Parr Instruments model 4749, Moline, IL, USA), at 150°C for 5 h; (ii) extraction of the wet gel and a six-step solvent exchange process (two washings per day) with a fresh solvent in order to remove any unreacted species; (iii) a six-step solvent exchange process (two steps per day) with liquid CO<sub>2</sub> to completely substitute the organic solvent with carbon dioxide, followed by a slow supercritical drying (<1 bar·min<sup>-1</sup>); (iv) pyrolysis of the preceramic aerogel-foam composite in flowing nitrogen atmosphere (300 STP cm<sup>3</sup>·min<sup>-1</sup>) at 1000°C for 1 h with a heating rate of 5°C·min<sup>-1</sup>.

Neat ceramic foam specimens were also prepared for the purpose of comparing the mechanical performances with that of the composite specimens (see Section 2.3 Characterization). Ceramization was performed on pretreated PPI 90 foams by following the same heat treatment utilized for composite samples (i.e., 1000°C-1h-5°C·min<sup>-1</sup> in nitrogen flow). Table 1 summarizes the prepared samples and the adopted labeling system.

## 2.3 | Characterization

The chemical structure of preceramic samples was evaluated by means of Fourier transform infrared spectroscopy (FT-IR) with a PerkinElmer Spectrum One FT-IR Spectrometer (PerkinElmer, Waltham, USA) in attenuated total reflectance mode with a resolution of 4 cm<sup>-1</sup>.

Microstructural characterizations were carried out using an Olympus DSX100 Opto-Digital Microscope (Tokyo, Japan) and a Zeiss Supra-40 field emission gun scanning electron microscope (FE-SEM) (Berlin, Germany) to observe the aerogel-foam interface and the effect of the solvent on the dimensions of the colloidal particles. Specific surface areas (SSAs) and pore size distributions were evaluated by means of N<sub>2</sub> physisorption at 77 K with a Micromeritics ASAP 2020 instrument. SSAs were calculated with the Brunauer-Emmet-Teller approach at P/P<sup>0</sup> < 0.3, while the total pore volume was defined with the Barrett-Joyner-Halenda method upon adsorption near the saturation point (P/P<sup>0</sup> = 0.99) by applying the Kruk-Jaroniec-Sayari correction. Nonlocal density functional theory (NLDFT) was adopted on each adsorption branch to calculate the pore volume of ceramic aerogels in the 0.8–80 nm range. Calculations were performed using the kernel for N<sub>2</sub> adsorption on porous silica with cylindrical pores. Skeletal densities were calculated using a Micromeritics AccuPyc II helium pycnometer. Tests were carried out at 23°C imposing a testing pressure of 1.58 bar (23 psig). Bulk density and porosity were geometrically determined on sets of at least three specimens per sample class, once the skeletal density was known.

Thermal diffusivity and conductivity were measured with a Netzsch 467 HyperFlash instrument on cylindrical specimens (diameter,  $d = 12.7$  mm). Measurements were carried out applying self-regulating pulse widths in the 0.6 to 1 ms range, a laser voltage of 250 V, and a spot amplitude of 11 mm. The penetration model was used to fit the output curve. Being the thermal expansion coefficient of amorphous SiC relatively small (ca. 4·10<sup>-6</sup> K<sup>-1</sup> at 500°C<sup>26,27</sup>),  $k$  calculation was performed imposing a density constant with temperature (see Table 2).

Measurements of specific heat,  $C_p$ , were performed from room temperature to 1000°C under argon atmosphere using a Quantum Design PPMS calorimeter.

The mechanical properties of ceramic composite samples and neat ceramic foams were evaluated via compression tests on sets of at least three cylindrical specimens per sample ( $d = 12$  mm, thickness,  $t = 5$  mm) with an Instron 4502 (Norwood, US), equipped with an Instron 2518–804 load cell (10 kN) and applying a compression speed of 0.8 mm·min<sup>-1</sup>. The excess aerogel matter

**TABLE 1** Labeling system utilized for the presented specimens. Note that, if not differently specified, these labels refer to samples ceramized at 1000°C in nitrogen.

Type of material	Preparation method	Synthesis solvent	Label
Polyurethane foam	Replica	–	PPI 90
Aerogel	Gelation of precursors mix + Supercritical Drying	Acetone	A_Aerogel
		Cyclohexane	C_Aerogel
		n-Hexane	N_Aerogel
Composite aerogel + foam	Replica + impregnation in precursors mix + gelation + supercritical drying	Acetone	A_P9
		Cyclohexane	C_P9
		n-Hexane	N_P9

Abbreviation: PPI, pores per inch.

**TABLE 2** Linear shrinkage ( $\Delta l/l_0$ ) values, bulk ( $\rho_b$ ) density, skeletal ( $\rho_s$ ) density, and porosity of neat aerogels and foams before and after heat treatment at 1000°C.

Component	Preceramic $\rho_b$ (g·cm <sup>-3</sup> )	Ceramic $\Delta l/l_0$ (%)	$\rho_s$ (g·cm <sup>-3</sup> )	$\rho_b$ (g·cm <sup>-3</sup> )	Porosity (%)
N-aerogel	0.09 ± 0.01	42.0 ± 1.3	1.85	0.30 ± 0.03	83.6
A-aerogel	0.08 ± 0.01	46.0 ± 1.0	1.94	0.20 ± 0.04	89.7
C-aerogel	0.14 ± 0.01	52.0 ± 1.4	1.93	0.70 ± 0.01	63.7
PPI90	0.03 ± 0.003	25.4 ± 1.0	2.47	0.14 ± 0.002	94.3

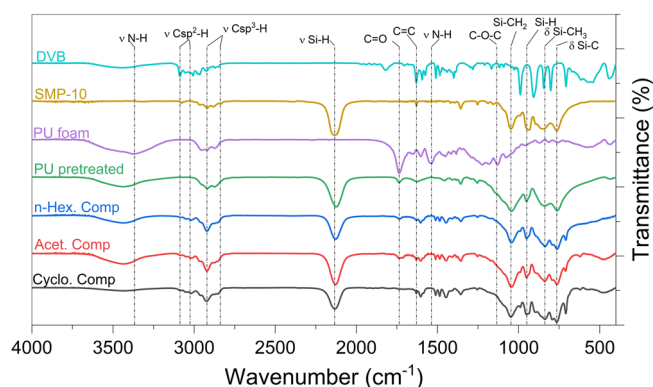


**FIGURE 1** Fourier transform infrared spectroscopy (FT-IR) spectra of precursors and preceramic aerogel/foam composites.

enveloping the foam as a consequence of the synthesis route was accurately removed before any mechanical test.

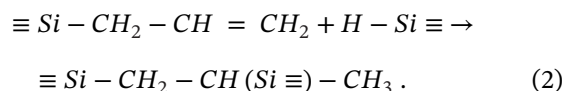
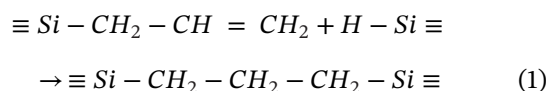
### 3 | RESULTS AND DISCUSSION

#### 3.1 | FT-IR characterization of preceramic samples

Infrared spectra of the preceramic samples (Figure 1) were acquired to observe the chemical bonds in these cross-linked polymers, prior to ceramization. In order to distinguish between the contributions of the different components of the system in the final FT-IR spectra, the

FT-IR of the as-received PU foam, pretreated PU/SMP-10 foam, pure SMP-10 and DVB reagents were reported as well. This clearly shows that the spectra of preceramic composites are generated as the superimposition of the spectra of the individual reagents and the components used in the architecture. Peaks relative to PU, such as C = O (1728 cm<sup>-1</sup>) and C-O-C (1128 cm<sup>-1</sup>) are visible in the pretreated foam even though degradation of the polymer starts below 300°C.<sup>28</sup> Moreover, the spectrum of pretreated PU foam shows peaks of Si-H, Si-CH<sub>2</sub>, Si-CH<sub>3</sub>, and Si-C bonds at 2130 cm<sup>-1</sup>, 1045 cm<sup>-1</sup>, 831 cm<sup>-1</sup>, and 760 cm<sup>-1</sup>, respectively, which can be assigned to the polycarbosilane.

In comparison with the spectrum of as-received SMP-10 (Figure 1, in yellow), the spectra of the foam/aerogel samples show that the relative height of the Si-H signal at 950 cm<sup>-1</sup> decreases with respect to the Si-CH<sub>2</sub> one as crosslinking takes place through hydrosilylation. In fact, silyl groups are consumed, and Si-CH<sub>x</sub> bonds are formed according to Equations 1 and 2:



Since Si-H groups are still present after pretreating the foam, a good adhesion with the aerogel is expected, since

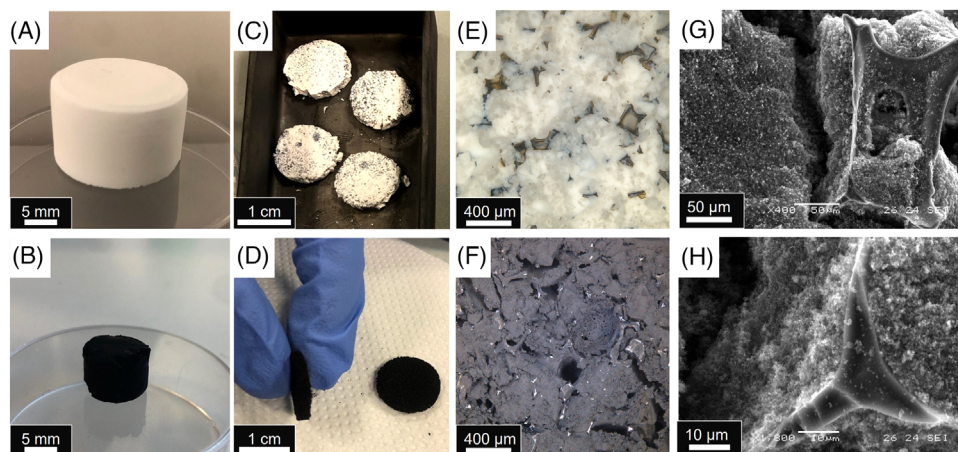


**FIGURE 2** Appearance of samples before and after pyrolysis at 1000°C: (A) preceramic C-aerogel; (B) ceramic C-aerogel; (C) preceramic composites; (D) ceramic composites; (E) preceramic composite from pores per inch (PPI) 90, using n-hexane as the solvent, featuring white preceramic aerogel and brownish pretreated foam struts; (F) PPI 90 composite after ceramization; (G and H) Scanning electron microscope details of a fracture surface in the ceramic A\_P9 sample, showing good adhesion at the aerogel/foam interface.

these bonds can undergo further crosslinking with vinyl bonds during the gelation step. Spectra of the preceramic composites synthesized in cyclohexane, n-hexane and acetone do not differ from each other, all of them featuring additional peaks in the 1330–1660  $\text{cm}^{-1}$  region that can be attributed to aromatic rings of divinyl benzene.

### 3.2 | Characterization of ceramic samples

Figure 2 shows the aerogel and the composite before and after the pyrolysis. From Figure 2A, B, it is clear that linear shrinkage is significant for aerogels, reaching 52% in case of cyclohexane-based neat aerogels (C-aerogel). At the same time, the usage of n-hexane (N-aerogel) and acetone (A-aerogel) leads to a linear shrinkage of 42% and 46%, respectively (see Table 2). On the other hand, the foams linearly shrink of about 25.4% upon pyrolysis (Table 2). This mismatch in shrinkage points out a manufacturing limit in attaining the final composite architecture: the aerogel partially retires, leaving behind macropores, which may limit the thermal insulation (Figure 2E, F). On the other hand, good interfacial adhesion between foam and aerogel should guarantee the mechanical stability of the composite. Figure 2G, H shows that cracks at the fracture surface tend to run preferentially through the aerogel bulk rather than at the aerogel/foam interface. A detail of the cross-section of the SiC foam in Figure 2H also provides an insight of the core of the struts. The absence of a hollowed core demonstrates that the replica was successfully synthesized. More details on the properties of polymer-derived SiC foams can be found elsewhere,<sup>24</sup> while some additional micrographs of the neat PPI90 foam are available in the [Supplementary Materials](#).

He pycnometry measurements revealed that the skeletal densities of ceramic aerogels range between 1.85 and 1.94  $\text{g}\cdot\text{cm}^{-3}$ , in line with similar PDCs found in the literature.<sup>29,30</sup> Considering that the density of amorphous SiC can be as low as 2.7  $\text{g}\cdot\text{cm}^{-3}$  (crystalline SiC has a density of 3.21  $\text{g}\cdot\text{cm}^{-3}$ ), it is clear that the degree of disorder in these amorphous aerogels is rather high even when taking into account the presence of free carbon domains owing to the use of DVB crosslinker.<sup>31,32</sup> As a matter of fact, the density of ordered graphite is 2.27  $\text{g}\cdot\text{cm}^{-3}$  and reaches higher values with the introduction of a certain degree of diamond-like  $\text{sp}^3$  carbon.<sup>33</sup> With respect to aerogels, ceramic foams present a higher skeletal density of 2.47  $\text{g}\cdot\text{cm}^{-3}$ , as a consequence of both the replica process and the absence of DVB in the precursors mix. The corresponding value of porosity of ceramic foams results equal to 94.3% when considering a bulk density of just 0.14  $\text{g}\cdot\text{cm}^{-3}$ .

The aerogels prepared using different organic solvents also present a large difference in terms of bulk density. The bulk density of C-aerogel is the highest both in the preceramic and ceramic form (i.e., 0.14 and 0.7  $\text{g}\cdot\text{cm}^{-3}$ , respectively). At the same time, that of N-aerogel and A-aerogel are lower. Such a large mismatch is in good agreement with the density difference observed for SiOC precursor aerogels synthesized in different solvents [23]. The difference in bulk densities of the preceramic aerogels suggests that, in a cyclohexane / SMP-10 system, the mutual solubility must be higher with respect to solvents such as n-hexane and acetone, implying that a higher fraction of cyclohexane is found in the wet gel before drying.<sup>34</sup> Therefore, cyclohexane-based aerogels would result more prone to structural shrinkage and further densification, as indicated by their higher bulk

**TABLE 3** Linear shrinkage, densities, and porosity of composite specimens after heat treatment (HT).

Solvent	Foam	Label	$\Delta l/l_0$ (%)	$\rho_b$ (g·cm <sup>-3</sup> )	$\rho_s$ (g·cm <sup>-3</sup> )	Porosity (%)
n-Hexane	PPI90	N_P9	23.4 ± 1.8	0.18 ± 0.20	1.96	90.8
Acetone	PPI90	A_P9	25.5 ± 0.8	0.21 ± 0.10	1.99	89.4
Cyclohexane	PPI90	C_P9	26.3 ± 1.5	0.21 ± 0.01	2.01	89.6

Abbreviation: DFT, density functional theory.

and skeletal density. The porosities calculated for each prepared aerogel (Table 2) clearly point to the same direction, reporting a low porosity of 63.7% in the case of C-aerogel, a porosity of 83.6% for aerogels synthesized in n-hexane (N-aerogel), and a maximum porosity of 89.7% for A-aerogel.

The density differences between the composites (reported in Table 3) and the stand-alone components can be discussed as follow. The skeletal density of N\_P9 samples is slightly lower than that of A\_P9 and C\_P9 samples. The bulk densities of composites fall between 0.18 and 0.21 g·cm<sup>-3</sup> and do not follow a trend when considering the  $\rho_b$  of aerogels. On the other hand, porosity values reach values around 90% in all the composite specimens.

The micrographs of ceramic aerogels given in Figure 3A–C show the substantial difference in the pore size as a function of the solvent utilized during the synthesis step. Specimens synthesized in n-hexane possess macropores in the range of hundreds of nm, the size of which gradually decrease when switching to acetone and cyclohexane. This can be indirectly observed when considering the shrinkage of the aerogel upon pyrolysis: aerogels synthesized in cyclohexane present a linear shrinkage of 52% versus values of 46% and 42% shown by samples originating from acetone and n-hexane, respectively. These results are confirmed by N<sub>2</sub> physisorption measurements of neat aerogels. Table 4 reports the SSAs and DFT pore volumes of preceramic aerogels, resulting in a maximum SSA of 1256 m<sup>2</sup>·g<sup>-1</sup> and a maximum volume of 4.84 cm<sup>3</sup>·g<sup>-1</sup> in the case of the C-Aerogel.

Figure 3D–F shows the nitrogen adsorption/desorption isotherms at 77 K of the pyrolyzed aerogels. The shapes of the three presented isotherms can be tentatively assigned to Type II/IV characteristics.<sup>35</sup> Such hybrid characterization is particularly clear for C-Aerogel. Type II isotherms are typically associated with macroporous sorbents, as confirmed by the SEM micrographs in Figure 3A–C, which highlight the presence of wide pores. Type IV isotherms, on the other hand, are mainly found in mesoporous structures (pore size in the 2–50 nm range), and present a hysteresis loop. This characteristic is prevalent in aerogels synthesized in cyclohexane, where most of the pore volume is given by mesopores in the 25–50 nm range (as confirmed by the steep slope step in the inset in Figure 3F). Such

**TABLE 4** Specific surface area and DFT pore volume of as-prepared ceramic aerogels synthesized using n-hexane, acetone, or cyclohexane.

Synthesis Solvent	n-Hexane	Acetone	Cyclohexane
Preceramic aerogels			
SSA (m <sup>2</sup> ·g <sup>-1</sup> )	552	447	1256
DFT Pore Vol (cm <sup>3</sup> ·g <sup>-1</sup> )	1.62	2.52	4.84
Ceramic aerogels			
SSA (m <sup>2</sup> ·g <sup>-1</sup> )	193	176	117
DFT Pore Vol (cm <sup>3</sup> ·g <sup>-1</sup> )	0.85	0.73	0.61
Ceramic composites			
Specimen	N_P9	A_P9	C_P9
SSA (m <sup>2</sup> ·g <sup>-1</sup> )	76	112	117
Pore Vol (cm <sup>3</sup> ·g <sup>-1</sup> )	0.26	0.15	0.34

Abbreviations: DFT, density functional theory; SSA, specific surface area.

samples also show a hysteresis loop resembling the H1 characteristic. Aerogels produced using n-hexane and acetone present a less pronounced hysteresis that extends to low partial pressures. Such a distinction arises as a result of the different pore size distributions, having these two aerogels a relevant fraction of macropores. Therefore, it is clear that the produced aerogels are characterized by different pore morphologies as a function of the different synthesis solvent.

In Figure 3A–C, one can observe the ceramized colloidal structure of the three aerogels, which is characterized by particles of 10–20 nm that aggregated into bigger clusters. Such microstructure derives directly from that of the preceramic aerogels, as these materials are synthesized via nucleation and growth of colloids from a liquid solution.

Specific surface area and pore volume values of the ceramic aerogels are summarized in Table 4 and show that the highest SSA of 193 m<sup>2</sup>·g<sup>-1</sup> is achieved by N-aerogel. On the other hand, pyrolyzed C-aerogel presents a SSA of 117 m<sup>2</sup>·g<sup>-1</sup> only. Such a drop in the specific surface area of the latter aerogel can be ascribed to the loss of a relatively high fraction of porosity with respect to the other two aerogels (insets in Figure 3D–F).

Adsorption-desorption isotherms at 77 K of N\_P9 and A\_P9 composite specimens (Figure 4) are characterized by H3 hysteresis loops and Type II curves, typical of macroporous sorbents.<sup>36</sup> With respect to the latter two samples,

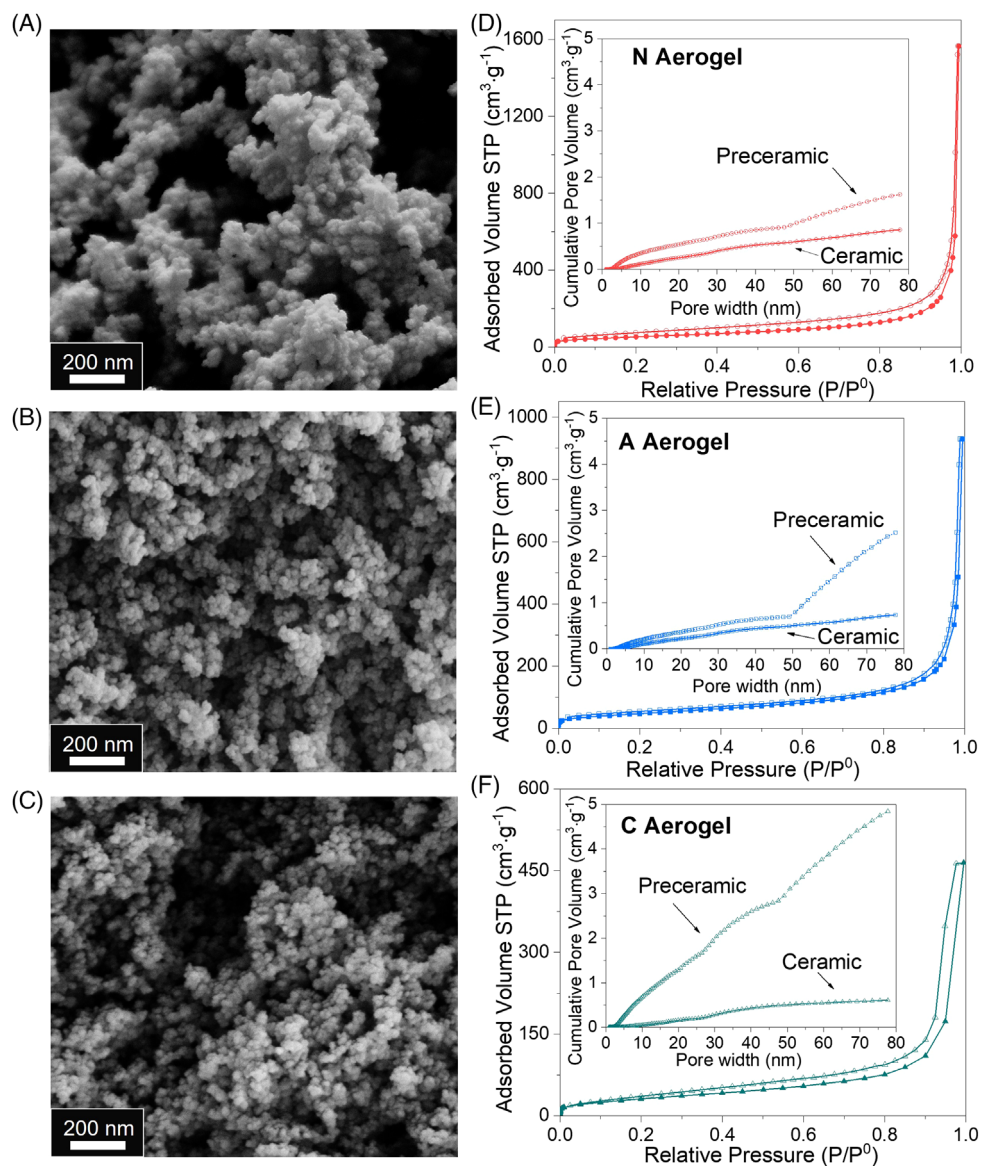


**FIGURE 3** Field emission gun scanning electron microscope (FE-SEM) micrographs and nitrogen physisorption isotherms at 77 K of ceramic aerogels prepared with different solvents: (A and D) n-Hexane; (B and E) acetone; (C and F) cyclohexane. Insets: comparison of density functional theory (DFT) cumulative pore volumes of preceramic and ceramic aerogels.

the hysteresis loop of C\_P9 shows a vague resemblance with the H2 category. For every case reported in Figure 4, the hysteresis loop extends in the low relative pressure region. The values of specific surface area and DFT pore volumes (Table 4) result comparably lower with respect to those of neat aerogels, especially in the case of N\_P9, as a consequence of the coupling of the aerogel with a dense structural component, such as the SiC foam. Only C\_P9 samples apparently preserve their SSA while losing almost half of the mesopore volume. These results are not in line with those of neat ceramic aerogels reported in Table 4 if an equal weight fraction of aerogel is assumed to be present in the pores of each composite. Such a deviation from the expected values could be explained by supposing

differences in the effective mass fraction of aerogels within the relative foam. Besides, ceramic replicas that undergo this synthesis procedure are usually affected by the presence of denser regions thus significantly influencing the calculation of SSA of weight-sensitive specimens such as those presented in this article.

Laser flash and specific heat ( $C_p$ ) measurements were carried out on promising composite samples (i.e., A\_P9 and N\_P9) to calculate their thermal conductivity ( $k$ ). The values of thermal conductivity and specific heat are given in Figure 5. The minimum  $k$  value of 0.041 W·m<sup>-1</sup>·K<sup>-1</sup> was obtained at 50°C for samples prepared using n-hexane (N\_P9), which further increased with the increase in the measurement temperature due to the

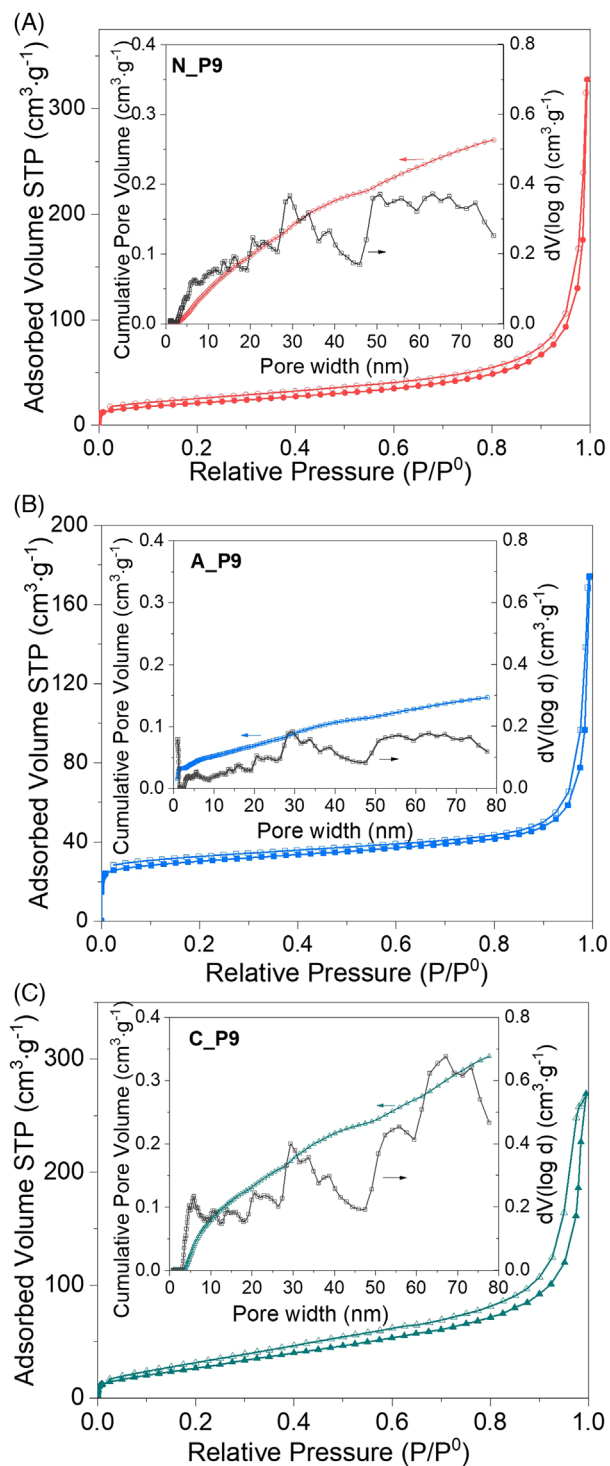


**FIGURE 4** N<sub>2</sub> physisorption isotherms at 77 K and pore volume distributions (insets) of ceramic composite specimens: (A) N\_P9 (red); (B) A\_P9 (blue); (C) C\_P9 (aqua green).

temperature dependence of specific heat. At a maximum temperature of 1000°C, N\_P9 responded with a  $k$  value of  $0.243 \text{ W}\cdot\text{m}^{-1}\text{K}^{-1}$ , lower than the corresponding value for A\_P9 (i.e.,  $0.276 \text{ W}\cdot\text{m}^{-1}\text{K}^{-1}$ ). Comparing these data with the available reports on bulk SiC, a clear insight on

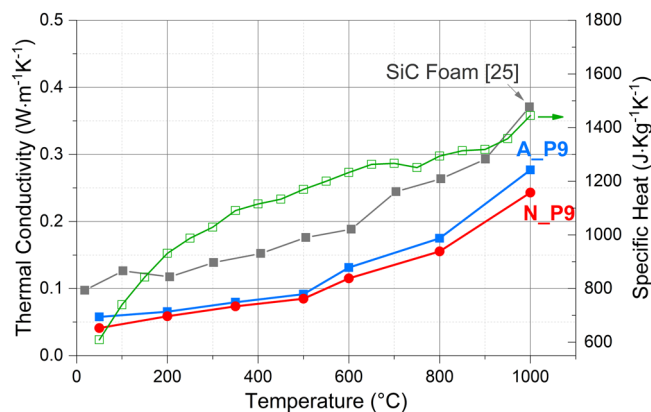


**FIGURE 5** Thermal conductivity of A\_P9 and N\_P9 compared to that of a neat SiC foam presented in ref. [25]. The specific heat of the SiC/C composites is also reported on the right axis.

the effect of porosity on thermal insulation properties is provided. As a matter of fact, crystalline and dense silicon carbide present  $k$  values that can exceed  $50 \text{ W}\cdot\text{m}^{-1}\text{K}^{-1}$  at 1000°C.<sup>37</sup> Available data on similar foams having partially closed cells can be considered for a comparison<sup>25</sup>: while aerogel-foam composites reported in this work do not exceed  $0.09 \text{ W}\cdot\text{m}^{-1}\text{K}^{-1}$  at 500°C and  $0.276 \text{ W}\cdot\text{m}^{-1}\text{K}^{-1}$  at 1000°C, unfilled foams obtained via impregnation of cellular PU structures with a polycarbosilane solution result in having a much higher conductivity of  $0.176 \text{ W}\cdot\text{m}^{-1}\text{K}^{-1}$  and  $0.371 \text{ W}\cdot\text{m}^{-1}\text{K}^{-1}$ , respectively. As can be easily noted, the addition of the aerogel is highly beneficial to the insulation performance. For instance, the thermal conductivity of N\_P9 turns out to be two-fold lower at 500°C.

The specific heat of aerogel/foam composites is depicted in Figure 5, showing a maximum value of  $1444.8 \text{ J}\cdot\text{Kg}^{-1}\text{K}^{-1}$  at 1000°C, in accordance with the theoretical values of silicon carbide.<sup>38</sup> The resulting combination of low thermal inertia and low thermal conductivity of these composites could be extensively exploited for high-temperature insulation, where a low density is required too.

The compressive stress-strain curves of the neat and the composite foams are presented in Figure 6. The compressive strength was calculated as the mean value of stress recorded on the plateau region of the serrated curves, after the stress build-up at a strain value over 20%. PPI90-derived replicas gave a compressive strength value of 0.24 MPa, similarly to other types of polymer-derived foams.<sup>39</sup> Loading the foams with aerogels seems to outdo the compressive strength values of the neat SiC foams (Table 5). The higher relative density of the composite structures might be one of the reasons causing such enhanced mechanical properties. A possibly stronger factor, assuming that the contribution of the aerogel to the strength of the composite is negligible, could be that the gelation at 150°C in diluted SMP-10 might have favored



**TABLE 5** Compressive strength values of ceramic foams and composites.

	Mean compressive strength (MPa)				
	Neat aerogels	Neat foam	Cyclohexane	Acetone	n-Hexane
PPI 90	0.04	0.24 ± 0.01	0.71 ± 0.04	0.77 ± 0.02	0.76 ± 0.03

Abbreviation: PPI, pores per inch.

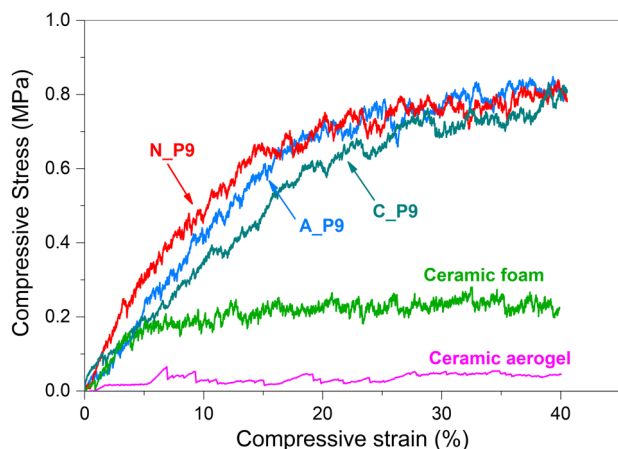


**FIGURE 6** Mechanical response of ceramic specimens: Neat pores per inch (PPI) 90 ceramic foam (magenta), C\_P9 (aqua green), A\_P9 (blue), N\_P9 (red).

its penetration into the partially swollen pretreated foam, thus leading to slightly thicker and stronger foam struts. In parallel, it is known that the presence of matter within a cellular structure tends to support the pore walls by homogenizing the load distribution during a compression event.<sup>40,41</sup>

## 4 | CONCLUSIONS

In this work, hierarchical porous structures obtained via polymer-derived and replica routes were presented. Specifically, amorphous silicon carbide replicas were reproduced from PU foams, and successfully adopted as a containment skeleton for polycarbosilane-derived silicon carbide aerogels.

The obtained architectures were produced using n-hexane, cyclohexane or acetone as synthesis solvent for the aerogel, resulting in hierarchically porous structures with different pore size distributions. Results of N<sub>2</sub> physisorption isotherms confirm that it is possible to indirectly manipulate this microstructural feature, achieving a meso-macroporous ceramic aerogel with a maximum SSA of 193 m<sup>2</sup>·g<sup>-1</sup> when using n-hexane.

For what concerns thermo-mechanical aspects, an optimal thermal conductivity of 243 mW·m<sup>-1</sup>K<sup>-1</sup> at 1000°C and 0.76 MPa of compressive strength were achieved in

the case of N\_P9. Besides, the incorporation of aerogels resulted with a beneficial effect on the mechanical properties of the ceramic foams. Given these results and the reduced processing-related shrinkage of the so-obtained aerogel, n-hexane can be suggested as the best of the three solvents for the synthesis of such architectures.


In conclusion, the presented composites might easily find applications in which high temperature insulation is essential, owing to the extremely low density of 0.18 g·cm<sup>-3</sup> coupled with a competitive thermal conductivity that is slightly affected by temperature dependence in the 50–1000°C range.

## ACKNOWLEDGMENTS

The authors would like to express their gratitude to Dr. Wenjie Xie and Dr. Lukas Pfeuffer for measurements of thermal diffusivity of specific heat, respectively. Thanks are also owed to Ms. Veronica Pallua and Ms. Giulia Avancini for their help in the making of the ceramic samples. Andrea Zambotti, Domenico Caputo, Gian Domenico Sorarù, and Mattia Biesuz acknowledge the financial support by the Italian Ministry of University and Research (MIUR) within the program PRIN2017 - 2017PMR932 “Nanostructured Porous Ceramics for Environmental and Energy Applications.” Cekdar Vakif Ahmetoglu would like to acknowledge the financial support of AFOSR with the program manager Dr. Ali Sayir through Grant #: FA9550-21-1-0279.


Open Access Funding provided by Universita degli Studi di Trento within the CRUI-CARE Agreement.

## ORCID

Andrea Zambotti  <https://orcid.org/0000-0002-8653-055X>

Emanuel Ionescu  <https://orcid.org/0000-0002-3266-3031>

Nicola Gargiulo  <https://orcid.org/0000-0001-7404-8056>  
Cekdar Vakifahmetoglu  <https://orcid.org/0000-0003-1222-4362>

Balanand Santhosh  <https://orcid.org/0000-0001-6060-3813>

Mattia Biesuz  <https://orcid.org/0000-0002-4338-4177>

Gian Domenico Sorarù  <https://orcid.org/0000-0002-0453-3379>

## REFERENCES

- Li B, Yuan X, Liao J, Mao B, Huang H, Wang X. Fabrication and characterization of a novel high-temperature vacuum insulation composites with SiC nanowire core material. *Mater Res Express*. 2019;6(9):095622. <https://doi.org/10.1088/2053-1591/ab1872>
- Bai S, Zhang N, Gao C, Xiong Y. Defect engineering in photocatalytic materials. *Nano Energy*. 2018;53:296–336. <https://doi.org/10.1016/j.nanoen.2018.08.058>
- Zera E, Brancaccio E, Tognana L, Rivoira L, Bruzzoniti MC, Sorarù GD. Reactive atmosphere synthesis of polymer-derived Si–O–C–N aerogels and their Cr adsorption from aqueous solutions. *Adv Eng Mater*. 2018;20(7):1–9. <https://doi.org/10.1002/adem.201701130>
- Pradeep VS, Ayana DG, Graczyk-Zajac M, Soraru GD, Riedel R. High rate capability of SiOC ceramic aerogels with tailored porosity as anode materials for Li-ion batteries. *Electrochim Acta*. 2015;157:41–5. <https://doi.org/10.1016/j.electacta.2015.01.088>
- Vakifahmetoglu C, Zeydanli D, Colombo P. Porous polymer derived ceramics. *Mater Sci Eng R Reports*. 2016;106:1–30. <https://doi.org/10.1016/j.mser.2016.05.001>
- Liang C, Wang Z, Wu L, Zhang X, Wang H, Wang Z. Light and strong hierarchical porous SiC foam for efficient electromagnetic interference shielding and thermal insulation at elevated temperatures. *ACS Appl Mater Interfaces*. 2017;9(35):29950–7. <https://doi.org/10.1021/acsami.7b07735>
- Liu Y, Chen Z, Zhang J, Ai S, Tang H. Ultralight and thermal insulation carbon foam/SiO<sub>2</sub> aerogel composites. *J Porous Mater*. 2019;26(5):1305–12. <https://doi.org/10.1007/s10934-019-00732-y>
- Su K, Wang Y, Hu K, Fang X, Yao J, Li Q, et al. Ultralight and high-strength SiCnw@SiC foam with highly efficient microwave absorption and heat insulation properties. *ACS Appl Mater Interfaces*. 2021;13(18):22017–30. <https://doi.org/10.1021/acsami.1c03543>
- Aly K, Lubna M, Bradford PD. Low density, three-dimensionally interconnected carbon nanotube/silicon carbide nanocomposites for thermal protection applications. *J Eur Ceram Soc*. 2021;41(1):233–43. <https://doi.org/10.1016/j.jeurceramsoc.2020.06.020>
- Colombo P. Conventional and novel processing methods for cellular ceramics. *Philos Trans R Soc A Math Phys Eng Sci*. 2006;364(1838):109–24. <https://doi.org/10.1098/rsta.2005.1683>
- Duan W, Yin X, Ye F, Li Q, Han M, Liu X, et al. Synthesis and EMW absorbing properties of nano SiC modified PDC-SiOC. *J Mater Chem C*. 2016;4(25):5962–9. <https://doi.org/10.1039/c6tc01142j>
- Colombo P, Mera G, Riedel R, Sorarù GD. Polymer-derived ceramics: 40 Years of research and innovation in advanced ceramics. *J Am Ceram Soc*. 2010;93(7):1805–37. <https://doi.org/10.1111/j.1551-2916.2010.03876.x>
- Eom JH, Kim YW, Raju S. Processing and properties of macroporous silicon carbide ceramics: a review. *J Asian Ceram Soc*. 2013;1(3):220–42. <https://doi.org/10.1016/j.jascr.2013.07.003>
- Aegerter MA, Leventis N, Koebel MM. *Aerogels handbook*. New York, NY: Springer; 2011. [https://doi.org/10.1007/978-1-4419-7589-8\\_4](https://doi.org/10.1007/978-1-4419-7589-8_4)
- Tychanicz-Kwiecień M, Wilk J, Gil P. Review of high-temperature thermal insulation materials. *J Thermophys Heat Transf*. 2019;33(1):271–84. <https://doi.org/10.2514/1.T5420>
- Ryzhenkov AV, Pogorelov SI, Loginova NA, Mednikov AF, Tkhabisimov AB. Radiant heat transfer reduction methods in heat insulation of power equipment. *Heat Transf XIV Simul Exp Heat Transf its Appl*. 2016;1(Ht):107–14. <https://doi.org/10.2495/ht160111>
- Vakifahmetoglu C, Semerci T, Gurlo A, Soraru GD. Polymer derived ceramic aerogels. *Curr Opin Solid State Mater Sci*. 2021;25(4):100936. <https://doi.org/10.1016/j.cossms.2021.100936>
- Santhosh B, Biesuz M, Sorarù GD. Thermal properties of dense polymer-derived SiCN(O) glasses. *Mater Lett*. 2021;288:129336. <https://doi.org/10.1016/j.matlet.2021.129336>
- Gurlo A, Ionescu E, Riedel R, Clarke DR. The thermal conductivity of polymer-derived amorphous Si–O–C compounds and nano-composites. *J Am Ceram Soc*. 2016;99(1):281–5. <https://doi.org/10.1111/jace.13947>
- Santhosh B, Vakifahmetoglu C, Ionescu E, Reitz A, Albert B, Sorarù GD. Processing and thermal characterization of polymer derived SiCN(O) and SiOC reticulated foams. *Ceram Int*. 2020;46(5):5594–601. <https://doi.org/10.1016/j.ceramint.2019.11.003>
- Rozenbaum O, De Sousa Meneses D, Echegut P. Texture and porosity effects on the thermal radiative behavior of alumina ceramics. *Int J Thermophys*. 2009;30(2):580–90. <https://doi.org/10.1007/s10765-008-0510-1>
- Vignoles GL, Ortona A. Numerical study of effective heat conductivities of foams by coupled conduction and radiation. *Int J Therm Sci*. 2016;109:270–8. <https://doi.org/10.1016/j.ijthermalsci.2016.06.013>
- Aguirre-Medel S, Jana P, Kroll P, Sorarù GD. Towards porous silicon oxycarbide materials: effects of solvents on microstructural features of poly(methylhydrosiloxane)/divinylbenzene aerogels. *Materials (Basel)*. 2018;11(12):2589. <https://doi.org/10.3390/ma1122589>
- Jana P, Zera E, Sorarù GD. Processing of preceramic polymer to low density silicon carbide foam. *Mater Des*. 2017;116:278–86. <https://doi.org/10.1016/j.matdes.2016.12.010>
- Santhosh B, Ionescu E, Andreolli F, Biesuz M, Reitz A, Albert B, et al. Effect of pyrolysis temperature on the microstructure and thermal conductivity of polymer-derived monolithic and porous SiC ceramics. *J Eur Ceram Soc*. 2021;41(2):1151–62. <https://doi.org/10.1016/j.jeurceramsoc.2020.09.028>
- Talwar DN, Sherbondy JC. Thermal expansion coefficient of 3C-SiC. *Appl Phys Lett*. 1995;67:3301. <https://doi.org/10.1063/1.115227>
- Hedayat A, Khounsary A, Mashayek F. Thermo-mechanical properties of silicon, germanium, diamond, beryllium and silicon carbide for high heat load x-ray optics applications. *Adv X-Ray/EUV Opt Components VII*. 2012;8502:850200. <https://doi.org/10.1117/12.929362>
- Ketata N, Sanglar C, Waton H, Alamercury S, Delolme F, Raffin G, et al. Thermal degradation of polyurethane bicomponent systems in controlled atmospheres. *Polym Polym Compos*. 2005;13(1):1–26. <https://doi.org/10.1177/096739110501300101>
- Zambotti A, Dorigato A, Sorarù GD, Fredi G, Valentini F. Low-temperature thermal energy storage with polymer-derived ceramic aerogels. 2022;20:39–50. <https://doi.org/10.1111/ijac.14158>
- Nguyen VL, Zera E, Perolo A, Campostrini R, Li W, Sorarù GD. Synthesis and characterization of polymer-derived SiCN aerogel.

- J Eur Ceram Soc. 2015;35(12):3295–302. <https://doi.org/10.1016/j.jeurceramsoc.2015.04.018>
31. Ruys AJ, Crouch IG. Siliconized silicon carbide. Amsterdam, Netherlands: Elsevier; 2021. <https://doi.org/10.1016/B978-0-08-102869-8.00007-0>
  32. Heera V, Prokert F, Schell N, Seifarth H, Fukarek W, Voelskow M, et al. Density and structural changes in SiC after amorphization and annealing. *Appl Phys Lett*. 1997;70(26):3531–3. <https://doi.org/10.1063/1.119223>
  33. Bhattarai B, Pandey A, Drabold DA. Evolution of amorphous carbon across densities: an inferential study. *Carbon N Y*. 2018;131:168–74. <https://doi.org/10.1016/j.carbon.2018.01.103>
  34. Hansen CM. Hansen solubility parameters: a user's handbook: Second edition. Boca Raton, FL: CRC Press; 2007. <https://doi.org/10.1201/9781420006834>
  35. Rouquerol F, Rouquerol J, Sing KSW, Llewellyn P, Maurin G. Adsorption by powders and porous solids. New York, NY: Academic Press; 2014
  36. Union I, Pure OF, Chemistry A. Reporting physisorption data for gas /solid systems with special reference to the determination of surface area and porosity. *Area*. 1985;57(4):603–19. <https://doi.org/10.1351/pac198557040603>
  37. Wei R, Song S, Yang K, Cui Y, Peng Y, Chen X, et al. Thermal conductivity of 4H-SiC single crystals. *J Appl Phys*. 2013;113(5):053503. <https://doi.org/10.1063/1.4790134>
  38. Román-Manso B, Chevillotte Y, Osendi MI, Belmonte M, Miranzo P. Thermal conductivity of silicon carbide composites with highly oriented graphene nanoplatelets. *J Eur Ceram Soc*. 2016;36(16):3987–93. <https://doi.org/10.1016/j.jeurceramsoc.2016.06.016>
  39. Semerci T, de Mello Innocentini MD, Marsola GA, Lasso PRO, Soraru GD, Vakifahmetoglu C. Hot air permeable pre-ceramic polymer derived reticulated ceramic foams. *ACS Appl Polym Mater*. 2020;2(9):4118–26. <https://doi.org/10.1021/acsapm.0c00734>
  40. Ashby MF. Mechanical properties of cellular solids. *Metall Trans A, Phys Metall Mater Sci*. 1983;14 A(9):1755–69. <https://doi.org/10.1007/BF02645546>
  41. Hubáľková J, Voigt C, Schmidt A, Moritz K, Aneziris CG. Comparative phenomenological study of fracture behavior of ceramic and glass foams under compressive stress using in situ X-ray microtomography. *Adv Eng Mater*. 2017;19(9):1–9. <https://doi.org/10.1002/adem.201700286>

## SUPPORTING INFORMATION

Additional supporting information can be found online in the Supporting Information section at the end of this article.

**How to cite this article:** Zambotti A, Ionescu E, Gargiulo N, Caputo D, Vakifahmetoglu C, Santhosh B, et al. Processing of polymer-derived, aerogel-filled, SiC foams for high-temperature insulation. *J Am Ceram Soc*. 2023;106:4891–4901. <https://doi.org/10.1111/jace.19118>